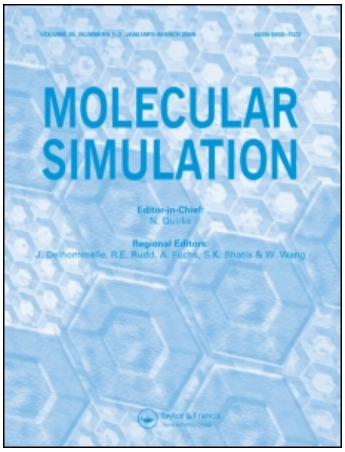

Molecular Simulation
Publication details, including instructions for authors and subscription information:
http://www.informaworld.com/smpp/title~content=t713644482

Lennard-Jones Mixtures in a Cylindrical Pore. A Comparison of Simulation and Density Functional Theory

Grant S. Heffelfinger[a]; Ziming Tan[a]; Keith E. Gubbins[a]; Umberto Marini Bettolo Marconi[ab]; Frank Van Swol[ac]
[a] School of Chemical Engineering, Cornell University, Ithaca, NY, USA [b] Permanent address: Dipartimento di Fisica, II Universita di Roma "Tor Vergata", Rome, Italy [c] Chemical Engineering Department, University of Illinois, Urbana, IL

To cite this Article Heffelfinger, Grant S. , Tan, Ziming , Gubbins, Keith E. , Marconi, Umberto Marini Bettolo and Van Swol, Frank(1989) 'Lennard-Jones Mixtures in a Cylindrical Pore. A Comparison of Simulation and Density Functional Theory', Molecular Simulation, 2: 4, 393 — 411
To link to this Article: DOI: 10.1080/08927028908034612
URL: http://dx.doi.org/10.1080/08927028908034612

Molecular Simulation, 1989, Vol. 2, pp. 393–411
Reprints available directly from the publisher
Photocopying permitted by license only

LENNARD-JONES MIXTURES IN A CYLINDRICAL PORE. A COMPARISON OF SIMULATION AND DENSITY FUNCTIONAL THEORY

GRANT S. HEFFELFINGER, ZIMING TAN, KEITH E. GUBBINS, UMBERTO MARINI BETTOLO MARCONI* and FRANK VAN SWOL**

School of Chemical Engineering, Cornell University, Ithaca, NY 14853 USA

(*Received February, 1988; in final form May, 1988*)

We report simulation results for binary Lennard-Jones mixtures in narrow cylindrical pores. The parameters are chosen to model an Ar-Kr mixture in a carbon dioxide pore. We focus on capillary condensation and locate this transition directly via a molecular dynamics simulation of two-phase coexistence. The chemical potentials in the pore are obtained via the particle insertion method. The latter results are used in a subsequent grand canonical Monte Carlo simulation in order to determine the bulk pressure, density and composition. We report density profiles and phase diagrams and compare the results with the local version of mean field density functional theory predictions for the same model. The simulation results for a mixture in which we neglect the size difference between Ar and Kr are compared with the non-local theory.

KEY WORDS: Lennard-Jones mixture, cylindrical pores, molecular dynamics, mean field theory.

INTRODUCTION

Over the last few years significant progress has been made in the understanding of fluid behaviour in the presence of substrates. In particular, a large amount of effort has been devoted to fluids in contact with single walls [1]. Both mean field density functional theory and computer simulation have been applied to the study of wetting and wetting transitions [e.g. 1–5]. The same two techniques have been used to investigate capillary condensation, a transition that is often in competition with wetting and layering transitions. Capillary condensation, the topic of this paper, occurs when a fluid is confined by a substrate [6–17]. The most common example is the vapour-liquid transition which, for a sufficiently attractive porous material, takes place at bulk undersatuarations [7]. This effect is of importance in industrial applications in such areas as oil recovery and phase separations. The macrosopic Kelvin equation [6], which is commonly used to locate the transition, is only applicable in the limit of large pores. For mesoporous materials this equation breaks down, since the fluid in narrow pores is extremely non-uniform and we cannot expect the notions underlying the Kelvin equation, such as uniform bulk phases and a sharp interface, to remain valid. Mean field density functional theory has proved successful in the description of capillary condensation. In its local form (LDA) it gives a qualitative description of the phase diagram, which can include wetting and prewetting transitions [7, 8]. The non-local extension of this theory was introduced by Tarazona [18], and replaces the

*Permanent address: Dipartimento di Fisica, II Universita di Roma "Tor Vergata", Rome, Italy.
**Present address: Chemical Engineering Department, University of Illinois, 1209 W. California Street, Urbana, IL 61801

local density by a smoothed density approximation (SDA). The SDA is superior, since it accounts realistically for the fluid structure which is typical of a fluid at high pressures in contact with substrate. This feature is missed by the LDA, which produces near monotonic density profiles. A detailed comparison of phase diagrams and density profiles for both LDA and SDA with simulation has recently been performed for a Lennard-Jones (LJ) fluid in a cylindrical pore [16, 17].

Although mean-field density functional theory for pure fluids in pores has received significant attention [7–11, 13, 16, 17], the theory has only recently been applied to mixtures in pores [15]. Mixtures in the presence of external fields were also studied by Evans and Marini Bettolo Marconi [11], and some preliminary simulations of Ar-Kr mixtures have been reported by Piotrovskaya and Smirnova [19]. Yeh et al. [20] have recently performed experiments on a mixture of ethanol and water in a porous sintered stainless steel plate and reported phase diagrams. We are not aware of any systematic experimental studies of mixtures in well characterized pores with a narrow pore size distribution similar to the experiments by Awschalom et al. [21], who considered pure fluids.

In this paper we report the results of molecular dynamics (MD) simulations for a LJ-mixture in cylindrical pores. In most of the simulations (Model I) the parameters are chosen to model an Ar-Kr mixture in a carbon dioxide pore. In particular, we locate the phase transition for two radii and two different mole fractions. The chemical potential of the two species is determined via the particle insertion method [22, 23], and the result is used in a grand canonical Monte Carlo (GCMC) simulation for a bulk mixture to determine the bulk composition of the 'reservoir' that is in equilibrium with the pore. We compare the results with the LDA for the same model. In addition, we present MD results for a second model mixture (Model II), namely that of equal-sized cores. By ignoring the size difference in the fluid-fluid interactions, we obtain a mixture that can also be treated in the SDA [24]. This allows us to investigate the influence of fluid structure. The SDA for the general case of a binary mixture with different core sizes is currently being developed [25].

This paper is arranged as follows. In section 2 we discuss the simulation methods and describe the particular model used. In section 3 we give a brief outline of the mean field theory. Finally, in section 4 we present the simulation and mean field results in the form of density profiles and phase diagrams and we discuss the comparison between the two approaches.

2. THE MODEL AND THE SIMULATION METHOD

The model binary mixture that we use in this work is identical to that studied by Tan et al. [15]. Briefly, the fluid interacts via a cut and shift LJ potential,

$$\phi_{ij}(r) = \begin{cases} \phi_{ij}^{LJ}(r) - \phi_{ij}^{LJ}(r_{ij}^c); & r \leqslant r_{ij}^c \\ 0; & r > r_{ij}^c \end{cases}$$

$$\phi_{ij}^{LJ}(r) = 4\varepsilon_{ij}\left[\left(\frac{\sigma_{ij}}{r}\right)^{12} - \left(\frac{\sigma_{ij}}{r}\right)^{6}\right] \qquad (1)$$

where r_{ij}^c denotes the cutoff distance of the ij-interaction, $r_{ij}^c = 2.5\sigma_{ij}$. The interactions between the fluid and the solid that makes up the porous material are simply represented by a one-body external field which only depends on the radial distance from the

axis of the cylinder. This particular form results when the fluid-wall interactions, which are taken to be a *full* LJ potential, are integrated over an infinite solid of uniform density $\rho_3\sigma_1^3$. The details of this integration have been presented previously [9, 15]. The final result for the external field is

$$V_i(r) = \pi\rho_3\varepsilon_{3i}\sigma_{3i}^3\left(\frac{\sigma_{3i}}{R}\right)^3\left[\frac{7}{32}\left(\frac{\sigma_{3i}}{R}\right)^6 I_9\left(\frac{r}{R}\right) - I_3\left(\frac{r}{R}\right)\right]; i = 1, 2 \quad (2)$$

with

$$I_n(x) = \int_0^\pi d\vartheta[-x\cos\vartheta + (1 - x^2\sin^2\vartheta)^{1/2}]^{-n} \quad (3)$$

where R denotes the pore radius, i.e. the distance at which the external field diverges.

For the first type of mixture studied, which we refer to as Model I, the LJ parameters for the two fluid components and the wall are chosen to model a mixture of Ar(1) and Kr(2) in a pore of solid CO_2(3):

$$\sigma_1 = 3.405\ \text{Å} \quad \sigma_2/\sigma_1 = 1.066 \quad \sigma_3/\sigma_1 = 1.1880$$
$$\varepsilon_1/k = 119.8\text{K} \quad \varepsilon_2/\varepsilon_1 = 1.3614 \quad \varepsilon_3/\varepsilon_1 = 1.6307 \quad (4)$$

The Lorentz-Berthelot mixing rules

$$\sigma_{ij} = (\sigma_i + \sigma_j)/2,\ \varepsilon_{ij} = \sqrt{\varepsilon_i\varepsilon_j};\ i, j = 1, 2, 3 \quad (5)$$

were used to determine the cross-parameters. The second mixture we consider, which we call Model II, differs from mixture I in only one respect, namely the size ratio of the fluid molecules. For this mixture we set $\sigma_2 = \sigma_1$ for the fluid-fluid interactions only. The wall-fluid collision diameters are the same as those of Model I. Note that by setting $\sigma_2 = \sigma_1$ both the attractions and repulsions are affected (see equation (1)). Of course, different schemes might be used to arrive at a reference fluid with spheres of equal size. For instance, one could just set the equivalent hard-sphere diameters equal rather than the σ-parameters. The equal-sized mixture can be treated in the SDA approximation, since this problem is a straightforward extension of the pure fluid [24].

The MD simulation method used in this work is similar to that applied in our earlier work [12, 16]. We use Verlet's Leap Frog algorithm in a modified form [26] to satisfy the constraint of constant temperature (T). The timestep used is $\Delta t = 0.005(m\sigma_1^2/\varepsilon_1)^{1/2}$. The NVT ensemble is extremely useful to investigate phase equilibria since it allows the direct simulation of two-phase coexistence. We have exploited this previously for the pure fluid [12, 16], and the results for the coexistence properties obtained via MD were shown to be in excellent agreement with those obtained from the independent route of thermodynamic integration. In this work we have taken the same approach, and studied the liquid-vapour equilibrium of the binary mixture through the simulation of the direct coexistence.

We have started from two equilibrated configurations of the two-phase pure fluid (Argon). These are characterized by $R^* = R/\sigma_1 = 2.5$ and $T^* = kT/\varepsilon_1 = 0.6$; and $R^* = 5$ and $T^* = 0.7$. We then changed the identity of a prescribed number of randomly chosen argon molecules to krypton. The *overall* mole fractions of argon in the pore we thus created were 0.5, 0.1 and 0. The latter case corresponds, of course, to pure krypton. The results for pure argon have already been published elsewhere [12, 13, 16]. The new configuration, that of a mixture, was then equilibrated until the effects of the starting configuration were removed, and then averages were accu-

mulated. Generally averages were accumulated for 300,000 timesteps for $R^* = 2.5$, and 20,000 timesteps for $R^* = 5$. The total number of molecules in the system was 356 for $R^* = 2.5$, and 1560 for $R^* = 5$.

The pore was divided radially and axially into bins, in order to determine the time average of the number of particles in each bin, thus allowing the calculation of the full density profile, $\rho_i(r,z)$ (see [12]). The bins each had a radial width of $\Delta r = 0.05\sigma_1$ and an axial length of $\Delta z = 0.2\sigma_1$. By randomly inserting test particles of both types (i.e. Ar and Kr) into the cylinder, and using the potential distribution theorem due to Widom [22, 23] we obtained the chemical potential profile $\mu_i(r,z)$ [12]. This profile can be averaged axially for the two separate regions, liquid and vapour [12]. At equilibrium the chemical potential of each species must have the same value in each phase. The chemical potentials (together with the temperature) fully characterize the bulk gas properties of the reservoir with which the pore is imagined to be in equilibrium. The bulk properties can then, in principle, be extracted by inverting an equation of state. Here we have instead used the two chemical potentials as input for a GCMC simulation, and directly simulated the bulk (gas) phase and thus obtained the bulk pressure $p^* = p\sigma_1^3/\varepsilon_1$, the bulk densities $\rho_1\sigma_1^3$ and $\rho_2\sigma_1^3$, and the bulk mole fractions.

3. MEAN FIELD DENSITY FUNCTIONAL THEORY

Consider a fluid-mixture at a fixed temperature T, and fixed chemical potentials μ_1 and μ_2, in a cylinder of radius R. The thermodynamic potential of interest is then the grand potential. The grand potential functional that we use is given by [27, 15],

$$\Omega[(\rho_1, \rho_2)] = F[(\rho_1, \rho_2)] + \sum_{i=1}^{2} \int d\mathbf{r}(V_i(\mathbf{r}) - \mu_i)\rho_i(\mathbf{r}) \tag{6}$$

where (ρ_1, ρ_2) denotes the two density profiles of species 1 and 2 and $F[(\rho_1, \rho_2)]$ is the Helmholtz free energy functional, which is commonly divided in two parts. The first part is due to the repulsions and the second part is due to the fluid-fluid attractions. By splitting up the fluid pair potentials in a WCA fashion and replacing the repulsive term by the equivalent term of a uniform hard sphere reference system at the local densities ρ_1 and ρ_2, we obtain the LDA,

$$F_{rep}[(\rho_1, \rho_2)] = \int d\mathbf{r} f_{HS}(\rho_1(\mathbf{r}), \rho_2(\mathbf{r})) \tag{7}$$

We follow Tan et al. [15] in our description of the equivalent (temperature dependent) hard sphere diameters, and further, we use the Percus-Yevick (PY) equation of state for the hard shpere mixture [28]. In the mean field approximation one ignores the correlations between the molecules, and hence the attractive term in (7) is written as,

$$F_{att}[(\rho_1, \rho_2)] = \frac{1}{2}\sum_{i,j} \iint d\mathbf{r} d\mathbf{r}' u_{ij}(|\mathbf{r} - \mathbf{r}'|)\rho_i(\mathbf{r})\rho_j(\mathbf{r}') \tag{8}$$

where u_{ij} represents the attractive part of the pair potential between molecules of species 1 and 2. The equilibrium density profile follows from minimizing the grand potential functional (6) with respect to the profiles. The coupled set of Euler-Lagrange equations that results from differetiating (6) with respect to $\rho_i(\mathbf{r})$ are solved numerically. Details of this procedure have been given previously (e.g. [27, 15]).

The LDA described above does not describe the oscillatory nature of the density profile. This is due to the local approximation (7). Tarazona [18] has extended the

LDA to a non-local theory by considering a repulsive free energy term that is a functional of a coarse-grained or smoothed density (SDA). The coarse-grained density $\bar{\rho}(\mathbf{r})$ is obtained by averaging over an appropriately chosen local volume centered at $\mathbf{r}$. A detailed description of the SDA for pure fluids can be found in references [18, 10, 16]. The generalization of the SDA, which is needed to describe mixtures of arbitrary size ratio, is currently being developed [25]. Here we will apply the pure fluid approach to a mixture for which the repulsive free energy contribution is given by that of a hard sphere mixture with a size-ratio of 1. A more detailed discussion of such a special mixture will be presented in a separate paper [24]. Briefly, we replace the hard sphere term in (7) by two terms. The first consists of the ideal gas contribution. The second term which we denote by ΔF_{HS}, contains the non-ideal contributions. For equal sizes we find [24],

$$\Delta F_{HS}[(\rho_1, \rho_2)] = \int d\mathbf{r}(\rho_1(\mathbf{r}) + \rho_2(\mathbf{r}))\Delta\psi_{HS}(\bar{\rho}_{tot}(\mathbf{r})) \tag{9}$$

where

$$\bar{\rho}_{tot}(\mathbf{r}) = \int d\mathbf{r}' w(|\mathbf{r} - \mathbf{r}'|; \bar{\rho}_{tot}(\mathbf{r}))(\rho_1(\mathbf{r}') + \rho_2(\mathbf{r}')) \tag{10}$$

and w denotes a normalized weight function [18, 10]. In the SDA we follow previous practice [16] and restrict ourselves to a temperature independent hard-sphere diameter, $d = \sigma_1$, and we use the Carnahan-Starling (CS) expression for the excess free energy per particle, $\Delta\psi_{HS}$,

$$\Delta\psi_{HS}(\bar{\rho}_{tot}) = kT\bar{\eta}(4 - 3\bar{\eta})/(1 - \bar{\eta})^2 \tag{11}$$

Here $\bar{\eta} = \frac{\pi}{6}\bar{\rho}_{tot}\sigma_1^3$. Again, the Euler-Lagrange equations that result for the SDA can be solved iteratively.

4. RESULTS AND DISCUSSION

We have examined two different pore radii, $R^* = 5$ at $T^* = 0.7$., and $R^* = 2.5$ at $T^* = 0.6$. For pure argon we have previously reported the phase diagrams of the confined fluid [16]. From this we know that both of the aforementioned conditions correspond to temperatures which are below the capillary critical temperature, which increases with the pore radius. Since the bulk critical temperature is higher for krypton (in units of ε_1), we also expect to be below the capillary critical temperature of the mixtures at the above mentioned temperatures. As described in section 2, we started our calculations from pure fluid configurations by randomly assigning the appropriate number of Kr molecules. The subsequent equilibration times can be quite long, as was previously noted by Lee et al. [27] who simulated free liquid-vapour interfaces for binary mixtures. Equilibrium is reached by diffusion of both species, and this is, of course a slow process. In principle one could speed the initial equilibration up by, for instance, randomly interchanging particles in a Monte Carlo procedure. We have not undertaken this in the calculations reported here. A quite difference approach would be to use the newly developed Gibbs Ensemble method for locating the phase transition [14, 29]. We checked that phase equilibrium was reached by inspecting the profiles $\mu_i(r, z)$ in both liquid and vapour regions. The profile should be fluctuating around the same constant value.

Table 1 Simulation results

		Model I. R = 5 and T* = 0.7*				
x_{ar}[†]	P*[‡]	x_1[§]	y_1[§]	y_{b1}[•]	μ_1/ε_1[§§]	μ_2/ε_1[§§]
0	0.11×10^{-3}	0	0	0	–	−4.4
0.1	0.15×10^{-2}	0.1	0.32	0.66	−6.2	−6.7
0.5	1.04×10^{-2}	0.47	0.90	0.96	−4.6	−6.8
1.0	2.00×10^{-2}	1	1	1	−4.1	–
		Model I. R* = 2.5 and T* = 0.6				
0	2.5×10^{-6}	0	0	0	–	−7.3
0.1	1.0×10^{-5}	0.09	0.67	0.82	−6.6	−7.5
0.5	4.0×10^{-5}	0.49	0.87	0.96	−5.7	−7.6
1.0	1.4×10^{-4}	1	1	1	−5.1	–
		Model II. R* = 5 and T* = 0.7 and $\sigma_2/\sigma_1 = 1$				
0.5	7.3×10^{-2}	0.48	0.93	0.93	−4.8	−6.6
		Model II. R* = 2.5 and T* = 0.6 and $\sigma_2/\sigma_1 = 1$				
0.5	0.4×10^{-4}	0.46	0.91	0.97	−5.7	−7.9

[†]Overall mole fraction of argon in the pore (equation (12))
[‡]Bulk pressure as obtained from GCMC
[§]Mole fraction of argon in liquid (gas) region of the pore (equation (14))
[•]Bulk mole fraction of argon as obtained from GCMC
[§§]Configurational chemical potential, $\mu_1 \equiv \mu_1 - 3kT\ln\Lambda_1$, as obtained via the particle insertion method

As discussed in section 2, by calculating the chemical potential of each fluid species in the pore, one can obtain the bulk properties of the reservoir in equilibrium with the pore via a GCMC simulation. The latter uses μ_1 and μ_2 as input. The resulting pressures, densities and compositions are summarized in Table 1. Here and below we shall find it convenient to refer to the different pores by their *overall* composition in the pore, which is simply defined as,

$$X_{ar} \equiv \frac{N_{Ar}}{N_{Ar} + N_{Kr}} \tag{12}$$

Here N_{Ar} and N_{Kr} denote the number of argon and krypton molecules in the pore. The physically relevant *bulk* compositions can be found in Table 1.

4.1 Fluid Structure

One method of examining liquid-gas coexistence is by investigating the structure of the non-uniform fluid-mixture in the pore, which is best illustrated by the full density profile of the fluid. Using a Silicon Graphics IRIS Workstation, the density profiles for both components of the mixture can be displayed with high resolution. In figures 1 and 2 we show the full density profiles for the two different radii at two different compositions. For clarity we have reflected the density profile through the z-axis, and we display the two component profiles side by side. These figures show the structure of the fluid. In the liquid the profile shows clear bands, which correspond to annuli with a high local density. The menisci are clearly visible, and we note that Argon is positively adsorbed onto the hemispherical liquid-vapour interface. In order to compare the structure of the two components in the fluid-pore system the density profiles must be examined more closely. In figures 3 and 4 we show the axial density profile

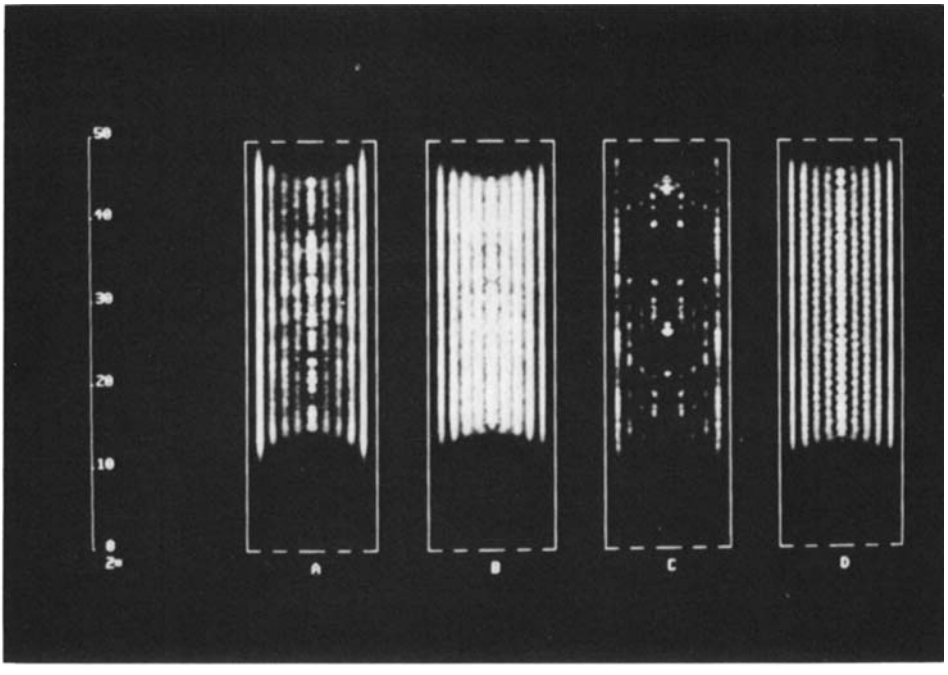

Figure 1 Density profile $\rho_i(r, z)$ for a mixture (Model I) in a cylindrical pore of radius $R/\sigma_1 = 5$ and a length $L/\sigma_1 = 50$, at a temperature $kT/\varepsilon_1 = 0.7$. For clarity we have reflected the profile through the z-axis. The composition of the left pair (A and B) is $x_{ar} = 0.5$ while that of the right pair (C and D) is $x_{ar} = 0.1$. For each pair, the left figure (A and C) represents argon and the right figure (B and D) represents krypton. (See colour plate X.)

for the different radii ($R^* = 5$ and $R^* = 2.5$ respectively) at both compositions. These profiles were produced by averaging the full density profile (figures 1 and 2) over the entire radius, according to

$$\rho_i(z) = \frac{2}{R^2}\int_0^R \mathrm{d}r r\rho_i(r, z) \tag{13}$$

The axial profiles show more clearly that for both radii at a value of $X_{Ar} = 0.5$, a thin layer of argon has adsorbed onto the krypton liquid meniscus surface. In addition, we note that for $X_{Ar} = 0.5$, the argon density is higher than that of krypton in the gas region but lower in the liquid region. This matches the mean-field density functional theory result of Tan et al. [15]. The structure can be examined more closely in the radial density profiles. These are obtained from the full density profile by performing an average over an interval (z_1, z_2), such that z_1 and z_2 are both either in the gas or liquid regions. We thus obtain the radial density profile in the gas and liquid regions, which we plot as a function of the radial distance r, measured from the pore axis. The results for both the gas and liquid regions and both compositions are displayed in figures 5 ($R^* = 5$) and 6 ($R^* = 2.5$). From figures 5b and 6b one can see that for $X_{Ar} = 0.5$, the argon peak at the wall in the gas phase is much higher than that of krypton. In figures 5d and 6d we show the radial density profiles for the gas regions for $X_{ar} = 0.1$. These profiles display poorer statistics due to the very small

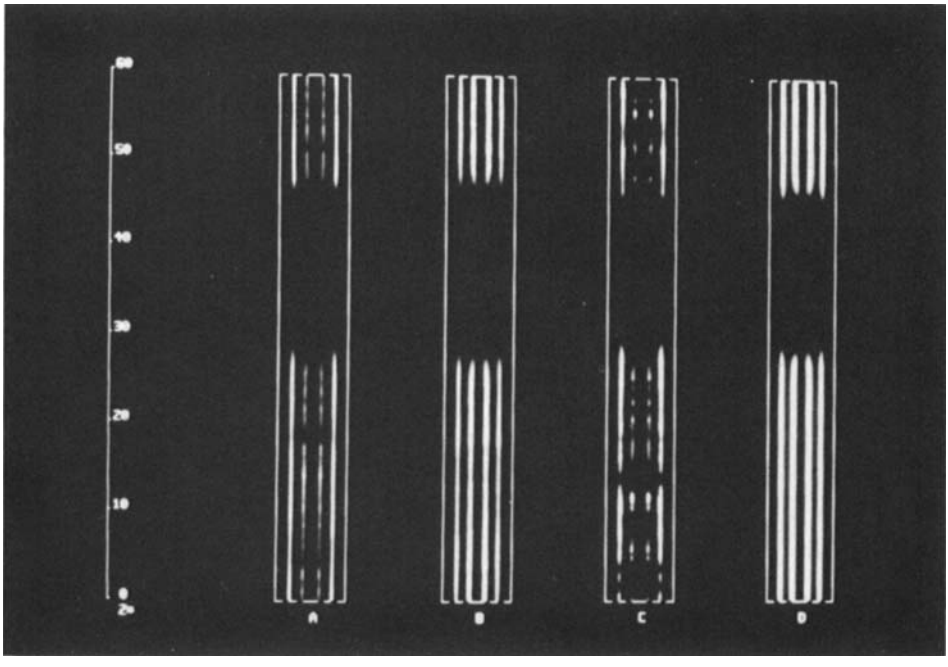

Figure 2 Density profile $\rho_i(r, z)$ for a mixture (Model 1) in a cylindrical pore of radius $R/\sigma_1 = 2.5$ and a length $L/\sigma_1 = 60$, at temperature $kT/\varepsilon_1 = 0.6$. For clarity we have reflected the profile through the z-axis. The composition of the left pair (A and B) is $x_{ar} = 0.5$ while that of the right pair (C and D) is $x_{ar} = 0.1$ For each pair, the left figure (A and C) represents argon and the right figure (B and D) represents krypton. (See colour plate XI.)

number of argon molecules present in the gas region. Also, note that for the $X_{AR} = 0.5$ mixtures, the argon peak near the wall in the liquid phase is higher than that of krypton despite the fact that the wall-krypton interaction is stronger (figures 5a and 6a).

By averaging the full density profiles both axially and radially over the 'bulk' regions, we determine an average density ρ_i^{av} (liq) and ρ_i^{av} (gas) for each species. From these we calculate the argon mole fractions in the pore, x_1 (liquid) and y_1 (gas), which we define as (cf [15])

$$x_1 \equiv \rho_1^{av}(\text{liq})/(\rho_1^{av}(\text{liq}) + \rho_2^{av}(\text{liq}))$$
$$y_1 \equiv \rho_1^{av}(\text{gas})/(\rho_1^{av}(\text{gas}) + \rho_2^{av}(\text{gas})) \quad (14)$$

We have collected the results in Table 1.

To compare the simulation and LDA we have performed the mean field (MF) calculations at the same relative temperature T/T_c. The values for the critical temperature of pure Argon, for the cut and shifted potential defined in equation (1) are $T_c^* = 1.11$ (simulation), $T_c^* = 1.2846$ (mean field plus PY), and $T_c^* = 1.2303$ (mean field plus CS). Since we do not have any simulation results for the critical temperature of pure argon, for the cut and shifted potential defined in equation (1), are we shall assume that the variation of T_c with composition is similar to that of the mean field result, that is,

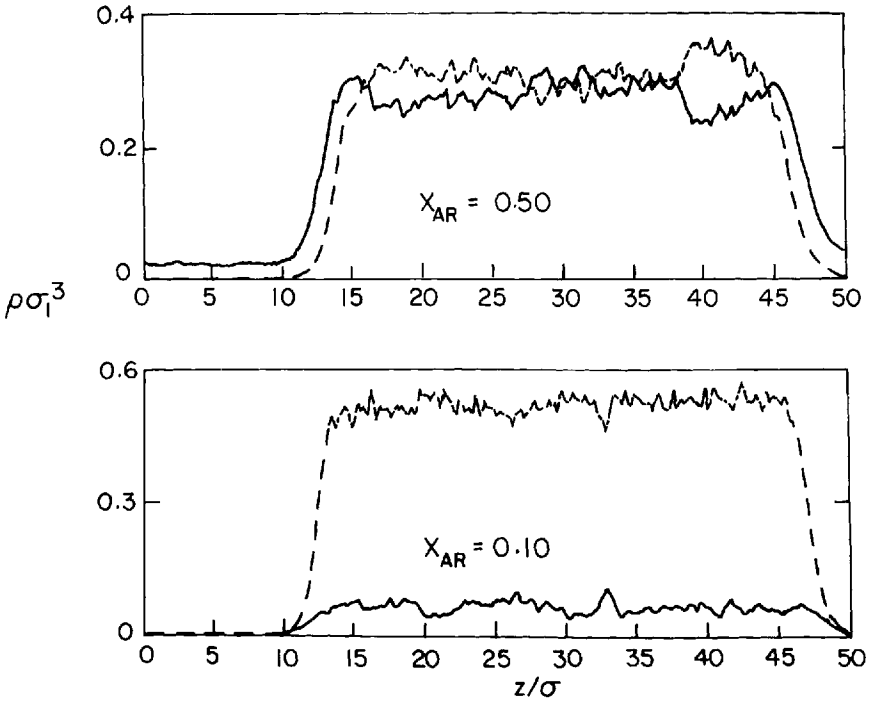

Figure 3 Axial density profile (see equation (13)) for $R^* = 5$, $T^* = 0.7$, $x_{ar} = 0.5$ (top) and 0.1 (bottom). Both liquid and gas regions are present. Argon is shown by a solid line and krypton by a dashed line. Argon is positively adsorbed onto the interface for $x_{ar} = 0.5$.

$$\frac{T_c^{MF}(y_b)}{T_c^{MF}(y_b = 1)} = \frac{T_c^{sim}(y_b)}{T_c^{sim}(y_b = 1)} \tag{15}$$

and thus we find the required MF temperature as

$$T^{MF} = T^{sim} \frac{T_c^{MF}(y_b = 1)}{T_c^{sim}(y_b = 1)} \tag{16}$$

Typical mean field results for the radial density profiles that we obtain using the LDA are shown in figures 7a and 7b, for $R^* = 5$ and $R^* = 2.5$ respectively. The profiles shown correspond to bulk gas densities of argon of $y_{bl} = 0.96$ (figure 7a) and $y_{bl} = 0.82$ (figure 7b), and can be compared directly to those of figures 5a and b and figures 6c and d respectively. As expected, the LDA profiles show none of the liquid structure that is present in the simulation. Also, the single peak in the gas is smaller than the simulation result. In contrast, the SDA does show liquid structure. This is clear from figure 8 where we present the SDA results for the equal-sized mixture (Model II) introduced in section 3. We compare the SDA directly with simulation at the respective phase transitions. The comparison between simulation and SDA is done by performing the MF calculation at the same value of y_{bl} as the simulation. The latter value is obtained from the chemical potentials and a subsequent GCMC run (see section 2). Variations in the chemical potentials will affect y_{bl}, and as can be seen

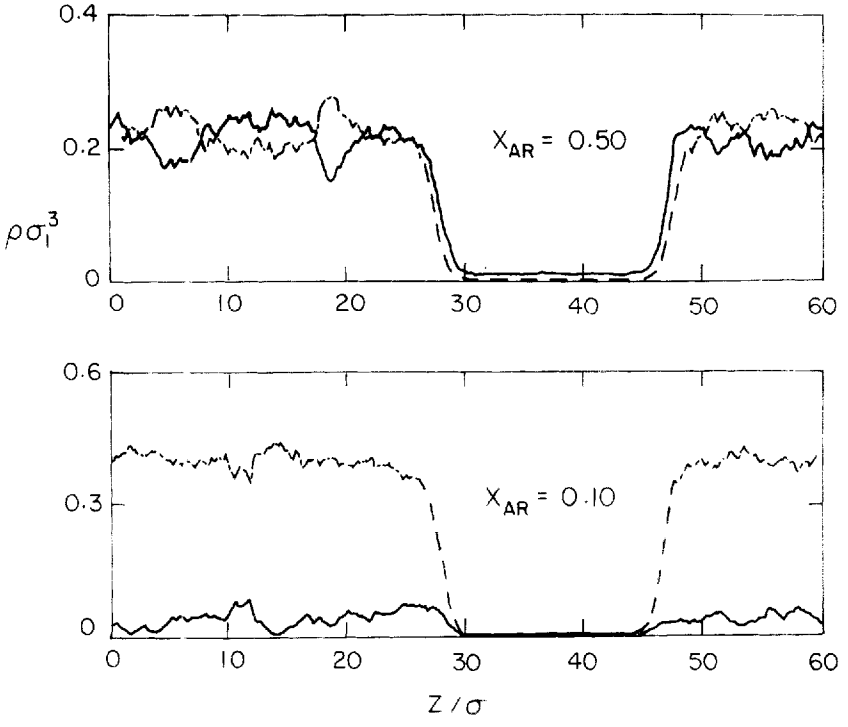

Figure 4 Axial density profile (see equation (13)) for $R^* = 2.5$, $T^* = 0.6$, $x_{AR} = 0.5$ (top) and 0.1 (bottom). Both liquid and gas regions are present. Argon is shown by a solid line and krypton by a dashed line. Argon is positively adsorbed on to the interface for $x_{AR} = 0.5$.

in figures 9b and 9d below, the liquid composition in the pore varies extremely rapidly with y_{b1} when the bulk is nearly pure Argon (i.e. $y_{b1} > 0.9$). Both of our simulations for equal-sized mixtures happen to correspond to $y_{b1} > 0.9$ (see Table 1), and we should thus be careful in comparing SDA with the simulation. Keeping this in mind, we conclude that the SDA seems to give a good description of the mixture, but further simulations at smaller values of y_{b1} are definitely needed to assess the accuracy of the SDA. It is worthy of note that the simulation profiles in figure 8 are also quite similar to those in figures 5 and 6. This indicates that the equal-sized mixture behaves very similarly to the more realistic Ar/Kr mixture (Model I), which has a size ratio $\sigma_2/\sigma_1 = 0.166$. Recall that the two models only differ in the fluid-fluid interactions. Although a full assessment of SDA for mixtures must await a more detailed systematic simulation study of mixtures in pores and in the bulk, we are encouraged by the good agreement found for the density profile of equal-sized mixture.

4.2 Phase Diagrams

In figures 9a and 9c we show the p-x_1-y_1 diagram, comparing simulation and LDA. We plot the bulk pressure versus the gas and liquid mole fractions of species 1 (Argon) in the pore. For comparison we include the MF result for the bulk (cf. Tan et al. [15]).

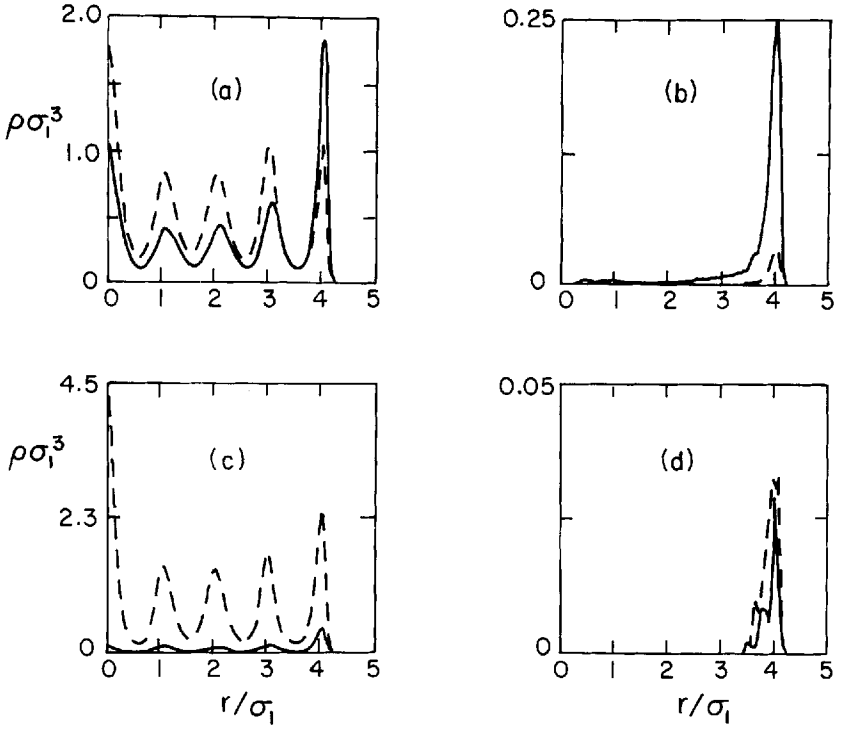

Figure 5 Radial density profiles for argon (solid lines) and krypton (dashed lines) in the liquid region (a and c) and gas region (b and d) of the fluid-pore system ($R^* = 5$). The top row corresponds to an overall composition of $X_{ar} = 0.5$, and the bottom has $X_{ar} = 0.1$.

The LDA shows a dramatic change upon confinement. The transition shifts to lower pressures, just as for the pure fluids [6-17]. The difference in gas and liquid compositions is much smaller in the pore than in the bulk. In figures 9b and 9d we plot the liquid and vapour composition for argon in the pore (equation (14)) versus the bulk composition in a x_l-y_l-y_{bl} diagram. Again, for the LDA we show the corresponding bulk liquid and vapour compositions as a reference. This figure illustrates that the gas composition is more affected by the confinement, the liquid remaining very close to the bulk line. This reflects the preferential adsorption for krypton in the gas phase [15]. The LDA in figures 7 and 9 produces results that are quite different from the simulation. This is most likely due to the difference in bulk phase diagrams combined with the rather crude nature of the local approximation. We note from our previous work on pure fluids that the LDA is only expected to show qualitative agreement with simulation, in contrast to SDA [16].

The relative adsorption of the two components, Γ_2/Γ_1, is shown in figure 10. Here the adsorption is defined by

$$\Gamma_i = \frac{1}{R}\int_0^R ds s\rho_i(s) - \frac{1}{2}R\rho_{bi}; \; i = 1,2 \tag{17}$$

where ρ_{bi} denotes the bulk density of species i. As noted before [15], the relative adsorption rises rapidly as y_{bi} is lowered. For the liquid phase the LDA again

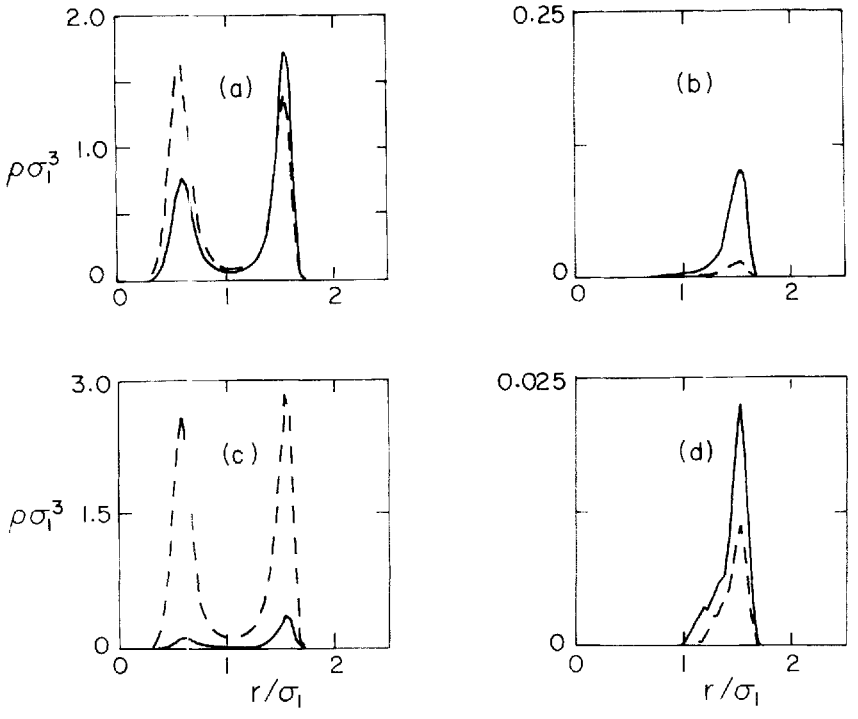

Figure 6 Radial density profiles for argon (solid lines) and krypton (dashed lines) in the liquid region (a and c) and gas region (b and d) of the fluid-pore system ($R^* = 2.5$). The top row corresponds to an overall composition of $X_{ar} = 0.5$, and the bottom has $X_{ar} = 0.1$.

underestimates the effect of confinement; for the gas phase LDA gives a result that is too low for $R^* = 5$ and somewhat too high for $R^* = 2.5$.

Acknowledgments

It is a pleasure to thank Brian K. Peterson for a copy of his GCMC program, and John Jackson for doing the photography. This work was supported by the Gas Research Institute, the Materials Science Center at Cornell University, and by a National Science Foundation US/Spain grant (CCB-8504023). It was also partially supported by the Army Research Office through the Mathematical Science Institute of Cornell University. The simulations were performed at the Cornell National Supercomputer Facility which is supported, in part, by the National Science Foundation and the IBM Corporation.

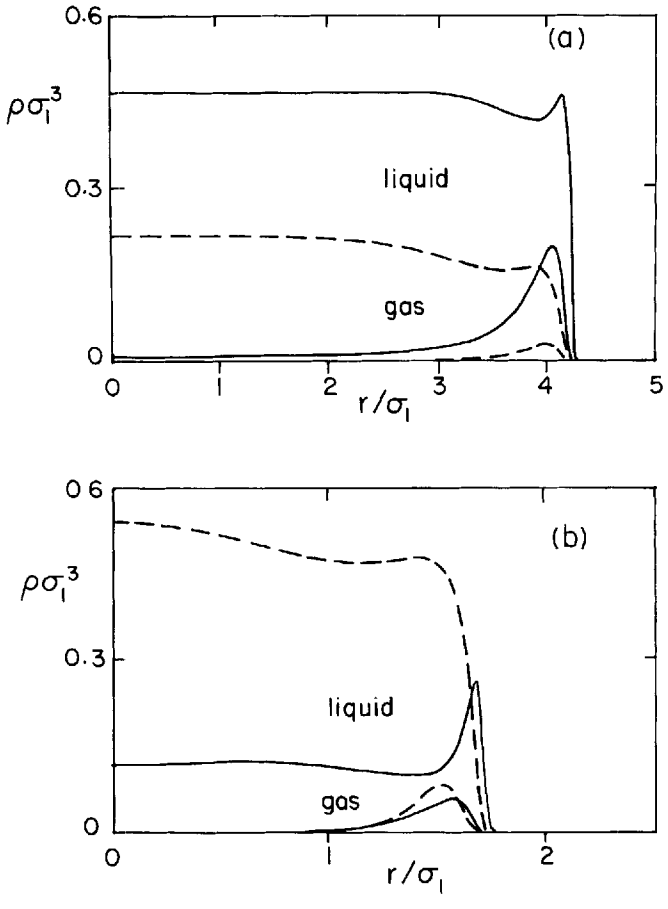

Figure 7 Radial density profiles for argon (solid lines) and krypton (dashed lines) as obtained by the mean field calculation using LDA. The gas and liquid profiles are shown at the transition. The results can be compared with the simulation results in figure 5 and figure 6. a) $R^* = 5$, $T^* = 0.7$ and $y_{bl} = 0.96$, b) $R^* = 2.5$, $T^* = 0.6$ and $y_{bl} = 0.82$.

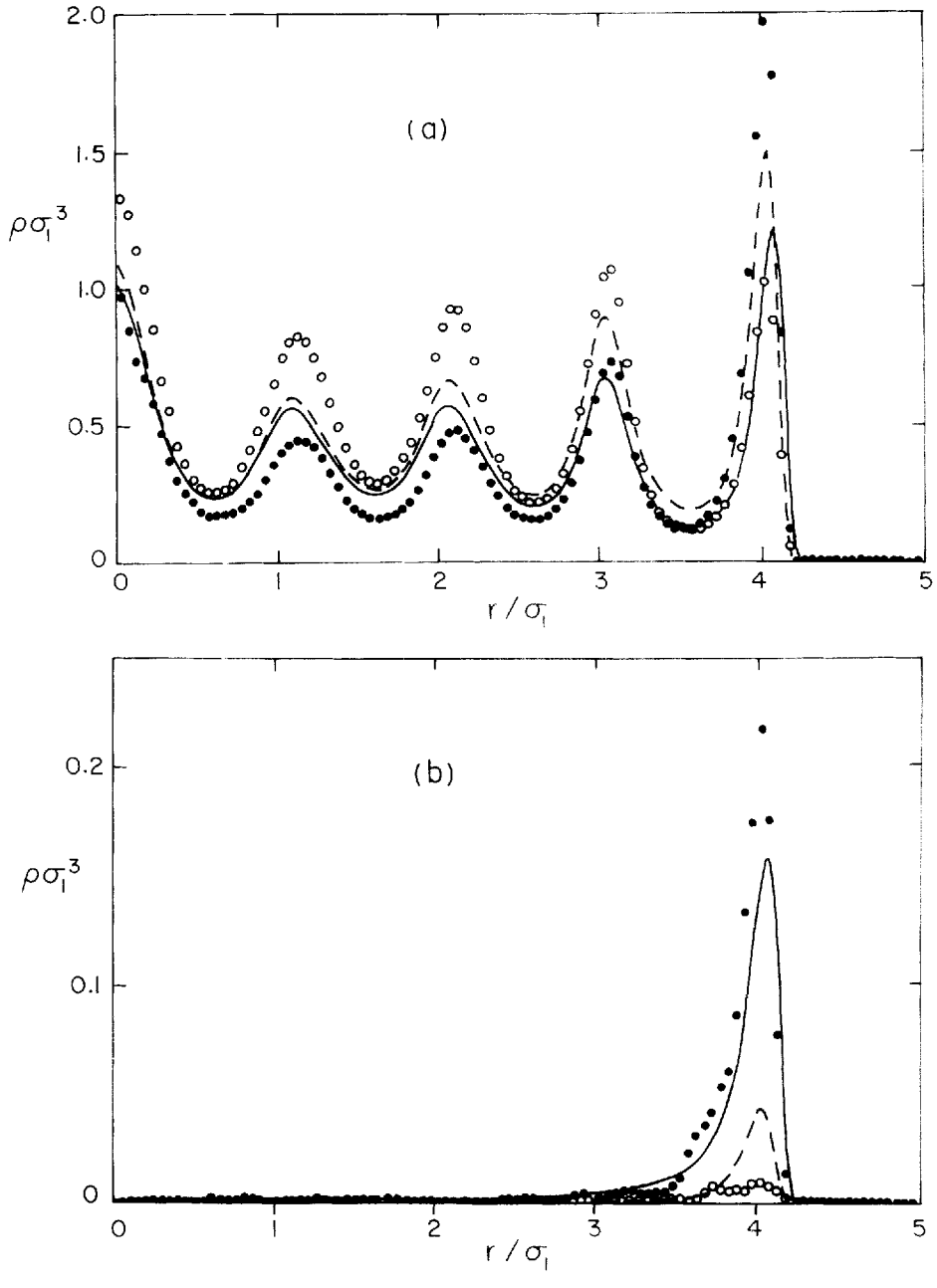

Figure 8 Radial density profiles for the equal-sized mixture (Model II) at the phase transition. Both gas and liquid profiles are shown. The simulation results are shown as symbols: filled circles (Argon) and open circles (krypton). The SDA profiles are shown as curves: solid lines (argon) and dashed lines (krypton). The top row (see also next page) corresponds to R* = 5, while the bottom row shows R* = 2.5, a) liquid, R* = 5, T* = 0.7 and $y_{kl} = 0.93$, b) gas, c) liquid, R* = 2.5, T* = 0.7 and $y_{kl} = 0.97$, d) gas.

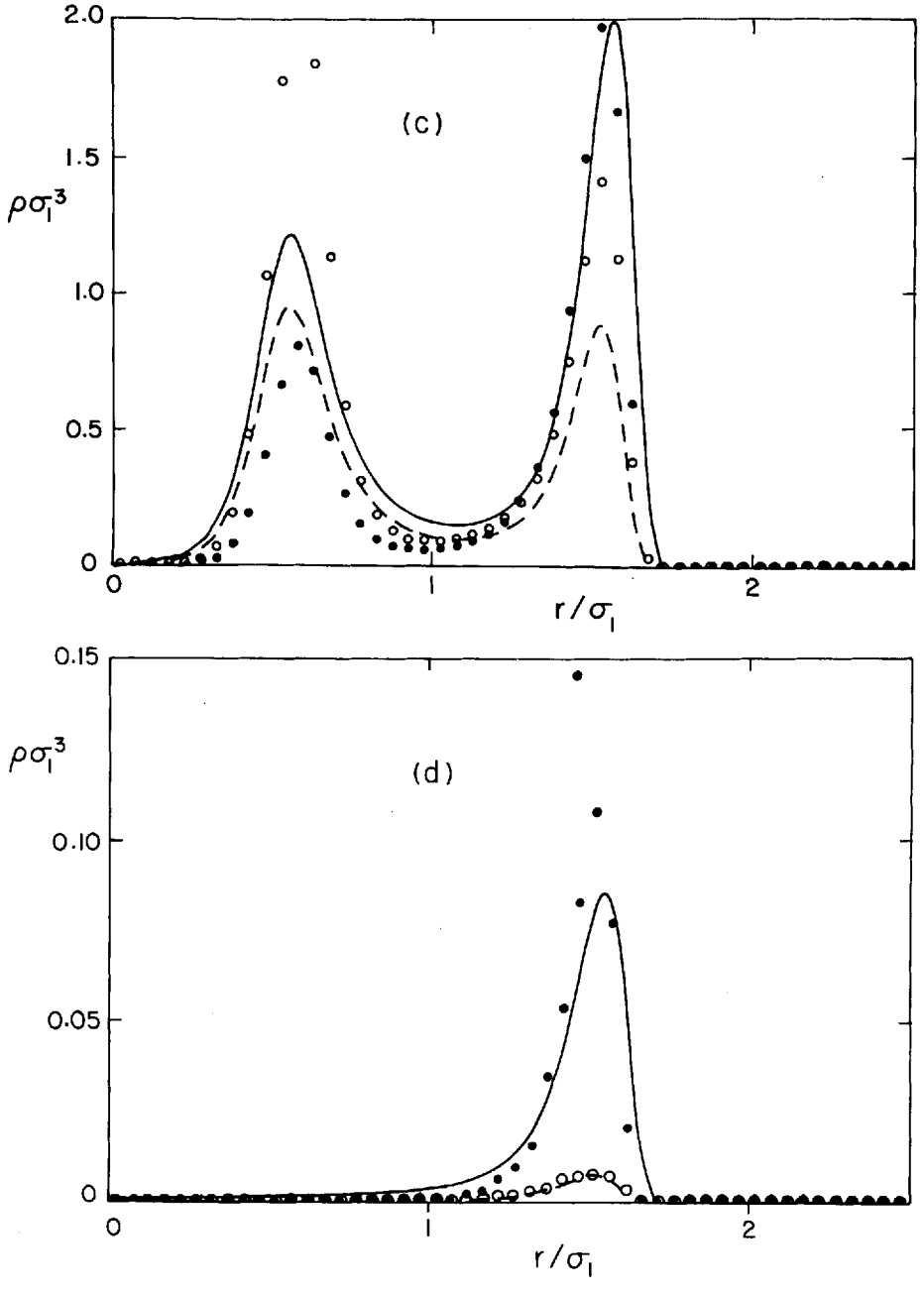

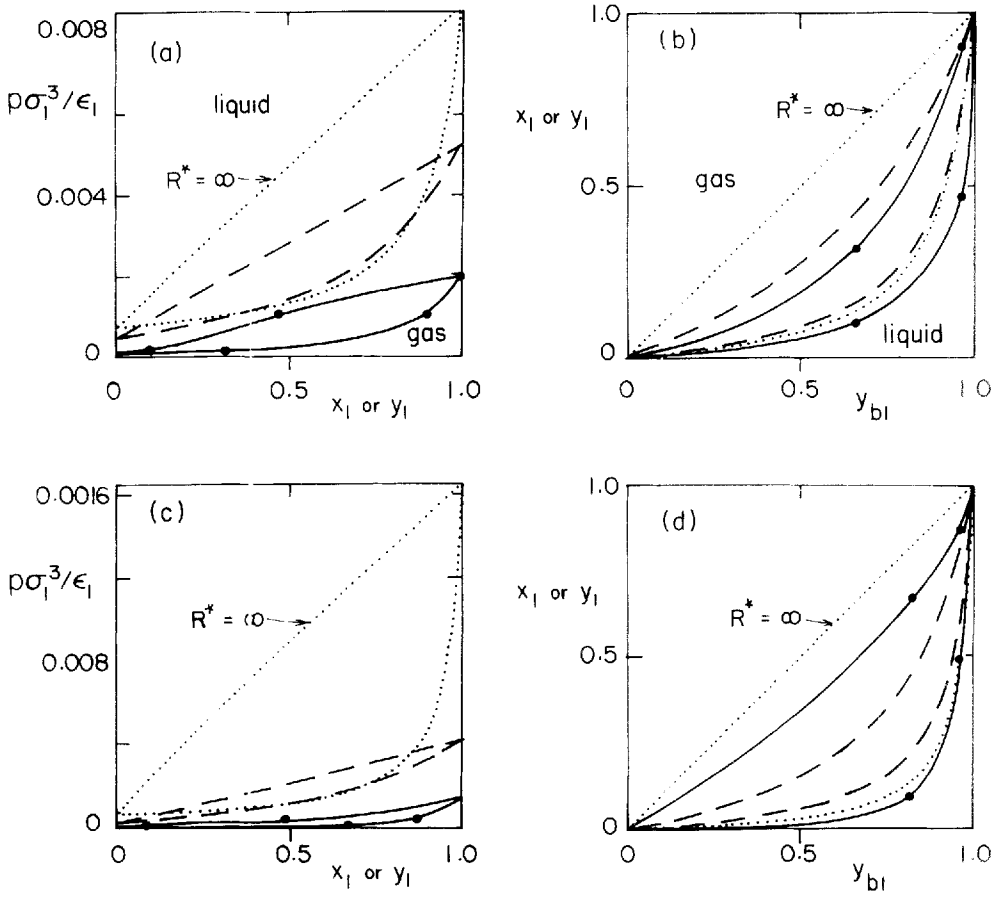

Figure 9 Capillary phase diagrams. Top row R* = 5, bottom row R* = 2.5. The curves denote the mean field results using the LDA. The dashed curves denote the results for the pore. The bulk result, which corresponds to R* = ∞, is shown for comparison (dotted lines). In the bulk case x_l and y_l denote x_{bl} and y_{bl} respectively. The MD results are shown as filled circles; the solid lines connecting them are intended as a guide to the eye.

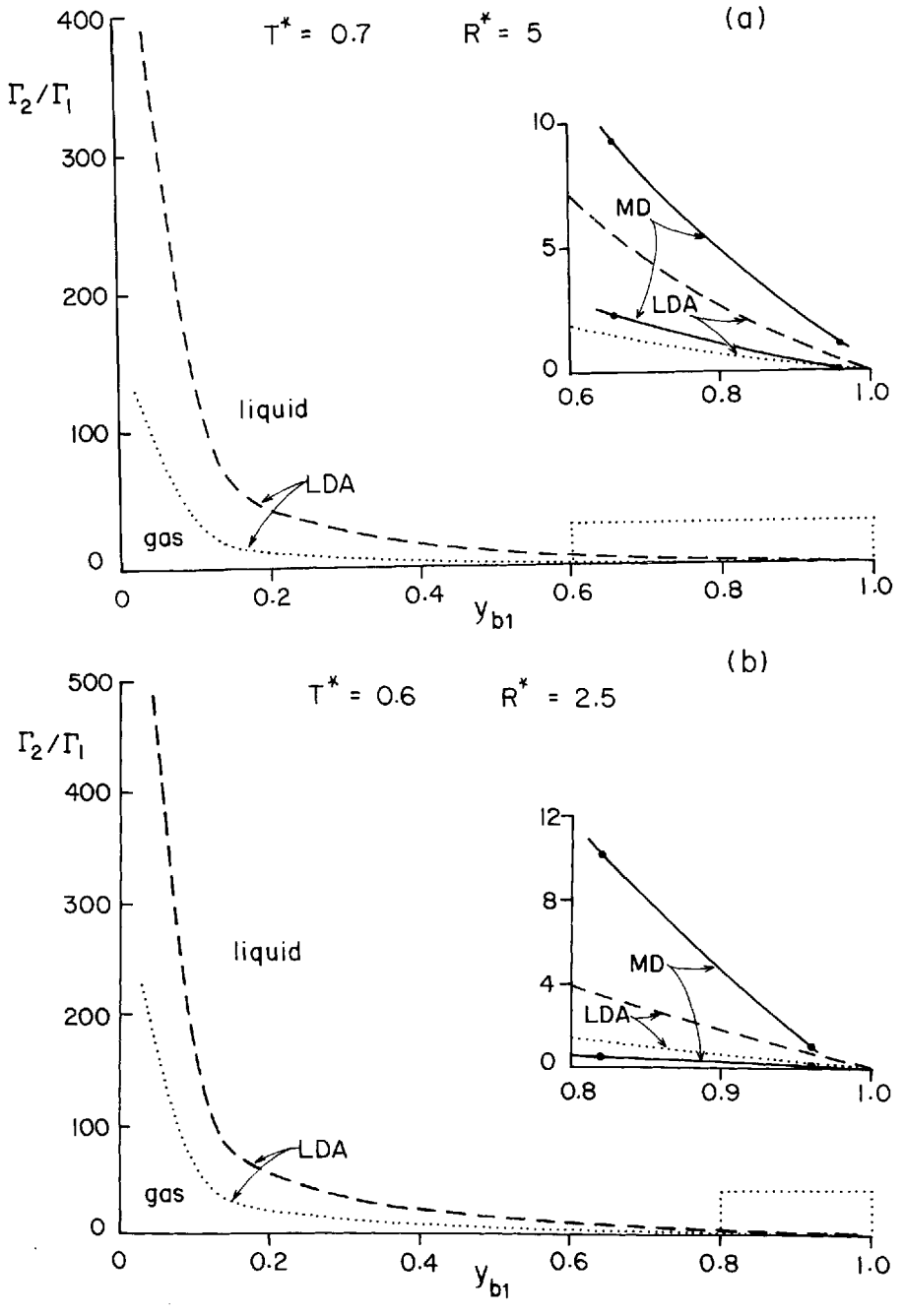

Figure 10 The relative adsorption of krypton relative to argon as a function of the bulk mole fraction of argon from simulation (points, solid lines) and LDA (---, liquid, and ..., gas), for coexisting gas and liquid phases (a) $R^* = 5$, $T^* = 0.7$, (b) $R^* = 2.5$, $T^* = 0.6$.

References

[1] For a review see: Sullivan, D.E. and Telo da Gama, M.M., in "Fluid Interfacial Phenomena," ed. C.A. Croxton (Wiley, New York), pp. 45-134 (1985).

[2] Tarazona, P. and Evans, R., "Wetting Transitions at Models of a Solid-gas Interface," *Mol. Phys.*,**48** ,799-831 (1983).

[3] Henderson, J.R. and van Swol, F., "On the Approach to Complete Wetting by Gas at a Liquid-Wall Interface: Exact sum rules, fluctuation theory and the verification by computer simulation of the presence of long range pair correlations at the wall," *Mol. Phys.*, **56,** pp. 1313-1356 (1985).

[4] van Swol, F. and Henderson, J.R., "Wetting at a Fluid-Wall Interface,"*J. Chem. Soc. Faraday Trans. 2*, **82,** pp. 1685-1699 (1986).

[5] Sikkenk, J.H., Indekeu, J.O., van Leeuwen, J.M.J. and Vossnack, E.O., "Molecular-Dynamics Simulation of Wetting and Drying at Solid-Fluid interfaces," *Phys. Rev. Lett.*, **59,** pp. 98-101 (1987). See also a comment on this paper, F. van Swol, *Phys. Rev. Lett.*, **60,** 239 (1988).

[6] Gregg, S.J. and Sing, K.S.W., "Adsorption, Surface Area and Porosity," 2nd edition (Academic Press, New York) (1982).

[7] Evans, R., Marini Bettolo Marconi, U. and Tarazona, P., "Fluids in Narrow Pores: Adsorption, Capillary Condensation and Critical Points," *J. Chem. Phys.*, **84,** pp. 2376-2399 (1986).

[8] Evans, R., Marini bettolo Marconi, U. and Tarazona, P., "Capillary Condensation and Adsorption in Cylindrical and Slit-like Pores," *J. Chem. Soc. Faraday Trans. 2*, **82,** pp.1763-1787 (1986).

[9] Peterson, B.K., Walton, J.P.R.B. and Gubbins, K.E., "Fluid Behavior in Narrow Pores," *J. Chem. Soc. Faraday Trans. 2*, **82,** pp. 1789-1800 (1986).

[10] Tarazona, P., Marini Bettolo Marconi, U. and Evans, R., "Phase Equilibria of Fluid Interfaces and Confined Fluids. Nonlocal Versus Local Density Functionals," *Mol. Phys.*, **60,** pp. 573-595 (1987).

[11] Evans, R. and Marini Bettolo Marconi, U., "Phase Equilibria and Solvation Forces for Fluids Confined Between parallel Walls," *J. Chem. Phys.*, **86,** pp. 7138-7148 (1987).

[12] Heffelfinger, G.S., van Swol, F. and Gubbins, K.E., "Liquid-vapour Coexistence in a Cylindrical Pore," *Mol. Phys.*, **61,** pp. 1381-1390 (1987).

[13] Peterson, B.K. and Gubbins, K.E., "Phase Transitions in a Cylindrical Pore. Grand Canonical Monte Carlo, Mean Field Theory and the Kelvin Equation," *Mol. Phys.*, **62,** pp. 215-226 (1987).

[14] Panagiotopoulos, A.Z., "Adsorption and Capillary Condensation of Fluids in Cylindrical Pores by Monte Carlo Simulation in the Gibbs Ensemble," *Mol. Phys.*, **62,** pp. 701-719 (1987).

[15] Tan, Z., van Swol, F. and Gubbins, K.E., "Lennard-Jones Mixtures in Cylindrical Pores," *Mol. Phys.*, **62,** pp. 1213-1224 (1987).

[16] Peterson, B.K., Gubbins, K.E., Heffelfinger, G.S., Marini Bettolo Marconi, U. and van Swol, F., "Lennard-Jones Fluids in Cylindrical Pores: Nonlocal Theory and Computer Simulation," *J. Chem. Phys.*, **88**, 6487 (1988).

[17] Ball, P. and Evans, R., "The Density Profile of a Confined Fluid: Comparison of Density Functional Theory and Simulation," *Mol. Phys.*, **63**, 159 (1988).

[18] Tarazona, P., "Free Energy Density Functional for Hard Spheres," *Phys. Rev. A*. **31**, pp. 2672-2679 (1985); see also ref. (10).

[19] Piotrovskaya, E.M. and Smirnova, N.A., "Monte Carlo Simulation of Lennard-Jones Fluids in Graphite Pores," preprint (1987).

[20] Yeh, G.C., Shah, M.S. and Yeh, B.V., "Vapor-liquid Equilibria of Nonelectrolyte Solutions in Small Capillaries. I. Experimental Determination of Equilibrium Compositions,"*Langmuir*, **2**, pp. 90-96 (1986).

[21] Awschalom, D.D., Warnock, J. and Shafer, M.W., "Liquid-film Instabilities in Confined Geometries," *Phys. Rev. Lett.*, **57,** pp. 1607-1610 (1986).

[22] Widom, B., "Some Topics in the Theory of Fluids," *J. Chem. Phys.*, **39**, pp. 2808-2812 (1963). An integrated version of the potential distribution theorem was recently suggested by U. Heinbuch and J. Fischer, "On the Application of Widom's Test particle Method to Homogeneous and Inhomogeneous Fluids," *Mol. Sim.*,**1**,109 (1987).

[23] Rowlinson, J.S. and Widom, B., "Molecular Theory of Capillarity," (oxford University Press) (1982).

[24] Marini Bettolo Marconi, U. and van Swol, F., "Structure and Phase Equilibria of Lenanrd-Jones Mixtures in a Cylindrical Pore. A Nonlocal Density Functional Theory," *Mol. Phys.*,submitted (1988).

[25] Tan, Z., Marini Bettolo Marconi, U., van Swol, F. and Gubbins, K.E., "Hard Sphere Mixtures Near a Hard Wall", *J. Chem. Phys.*, submitted (1988).

[26] Brown, D. and Clarke, J.H.R., "A Comparison of Constant Energy, Constant Temperature and

Constant Pressure Ensembles in Molecular Dynamics Simulations of Atomic Liquids," *Mol. Phys.*, **51**, pp. 1243-1252 (1984)

[27] Lee, D.J., Telo da Gama, M.M. and Gubbins, K.E., "The Vapour-liquid Interface for a Lennard-Jones Model of Argon-Krypton Mixtures," *Mol. Phys.*, **53**, pp. 1113-1130 (1984)

[28] Reed, T.M. and Gubbins, K.E., "Applied Statistical Mechanics," (McGraw-Hill, New York) (1973).

[29] Panagiotopoulos, A.Z., Quirke, N., Stapleton, M. and Tildesley, D.J., "Phase Equilibria by Simulation in the Gibbs Ensemble: Alternative Derivation, Generalization and Application to Mixture and Membrane Equilibria," *Mol. Phys.*, **63**, 527 (1988).